EPJ Web of Conferences **214**, 02021 (2019) https://doi.org/10.1051/epjconf/201921402021
CHEP 2018

Tracking system performance of the BM@N experiment

Mikhail Kapishin[1], *Vasilisa* Lenivenko[1], *Vladimir* Palichik[1], *Gleb* Pokatashkin[1], *Igor* Rufanov[1], *Veronika* Vasendina[1], *Nikolay Voytishin*[1,*], and *Alexander* Zinchenko[1]

[1]Joint Institute for Nuclear Research, Joliot Curie 6,141980 Dubna, Moscow region, Russia

Abstract. The Baryonic Matter at Nuclotron (BM@N) experiment represents the first phase of the Nuclotron-based Ion Collider Facility (NICA), a mega-science project at the Joint Institute for Nuclear Research. It is a fixed target experiment built for studying nuclear matter in conditions of extreme density and temperature. The tracking system of the BM@N experiment consists of three main detector systems: Multiwire Proportional Chambers situated before the magnet, Gas Electron Multipliers placed inside the magnet and Drift Chambers placed after the magnet. These systems provide the reconstruction of charged particles' trajectories and their momentum in the magnetic field. This information is further used by Time of Flight detectors for the particle identification procedure. The system's performance is reviewed and the spatial resolutions along with efficiencies of the detectors are estimated using the data collected in the recent physics runs of the Nuclotron.

BMN experimental setup out

The experimental setup of the BM@N experiment [1] contains a wide variety of detector systems used for the reconstruction of the passing particle trajectories as well as for their identification and estimation of some of their properties.

The trigger detectors system is situated before the analyzing magnet. Its main role is to trigger and reconstruct the initial time (T0) for the rest of the detectors and monitor the beam. Along with this, Multi-Wire Proportional Chambers (MWPC) are used for beam monitoring and particles' trajectory reconstruction in the area before the analyzing magnet. The central tracker is situated inside the magnet and consists of a silicon detector and a group of Gas Electron Multipliers (GEM) detector planes. The outer tracker consists of two drift chambers (DCH). The outer tracker is used for linking tracks from the central tracker with the Time of Flight (ToF) system. There are two ToF stations in the current experimental setup. The first one is situated between the last GEM plane and the first DCH and the second one is placed between the two drift chambers. The two ToF stations are used for particle identification and have different positions and sensitive aperture. The downstream of the experimental setup contains two calorimeters. The zero-degree

* Corresponding author: nvoytish@jinr.ru

calorimeter is used for measuring the centrality of nucleon-nucleon collisions. The electromagnetic calorimeter is used for the study of processes of γ, e+e- formation.

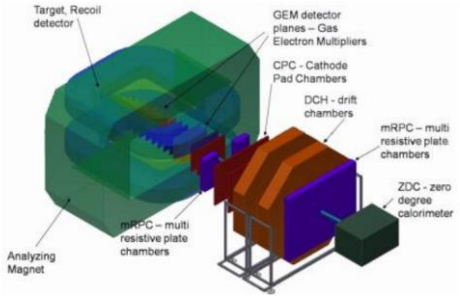

Fig. 1. BM@N experimental setup.

MWPC

The first tracking detector system intersected by the Nuclotron beam is the MWPC. The MWPC system consists of two chambers. Each MWPC [2] has 6 planes: two with wires oriented at angle of 0° and defined as X-planes, two with wires at angle of -60° defined as U-planes and two with wires at angle of 60° defined as V-planes. The wire pitch is 2.5 mm. All planes have high reconstruction efficiency, as shown in Fig. 2.

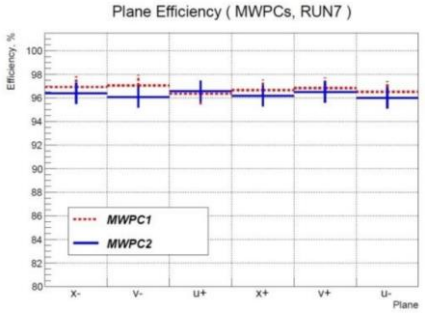

Fig. 2. MWPC efficiency per plane. Inefficiency for particular plane means the absence of the hit from this plane on the segment.

Drift Chambers

The two DCH detectors used in the experimental setup were originally part of the decommissioned NA48 experiment [3]. They form the outer tracker. Each drift chamber consists of four pairs of coordinate planes. Subsequent pairs have their wires positioned at angles of 0°, 90° and ±45°. The wire pitch is 10 mm for each. The sense wires of the planes from a particular pair are staggered by a half of a wire pitch in order to resolve the right-left ambiguities while reconstructing the coordinate.

The reconstruction algorithm developed consists of three main steps:

- coordinate reconstruction from fired wires;
- segment reconstruction in a particular chamber;
- global track reconstruction from segments in both chambers.

The reconstruction of a coordinate on a particular plane is done using a transfer function that converts the drift time in nanoseconds decoded from the digitized data into distance from the sensitive wire. This procedure is depicted in Fig. 3.

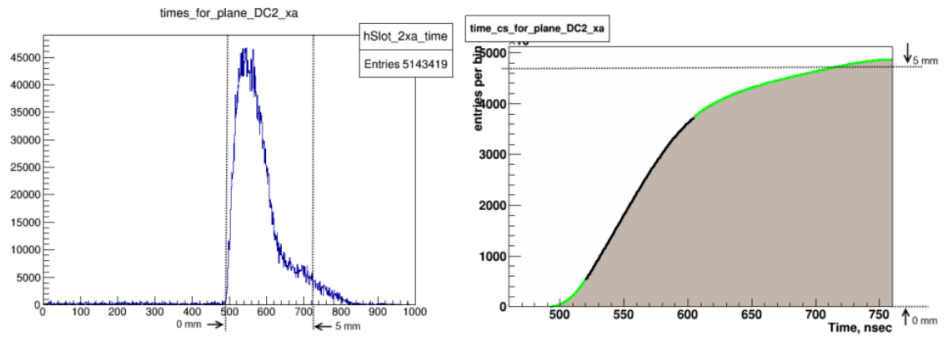

Fig. 3. Time distribution for a particular layer of a DCH (left). Integral form of the time distribution for a particular layer of a DCH (right).

The low edge of the time distribution (marked by the first dotted line) corresponds to particles that passed very close to the wire. We consider it as a start of our 5 mm distance between the sensing and field wire. We choose a time window that corresponds to the defined distance. The particles that gave the signal at the times corresponding to the upper edge of this window (second dotted line) are considered as having passed at the maximum distance from the sense wire. All particles that have the signal time outside the time window are not considered in further reconstruction steps.

The time distribution histogram (left side of Fig. 3) is transformed into its integral form (right side of Fig. 3) out of which the transfer function can be made. The transfer function converts the time value into the distance from the wire at which the particle passed the particular layer. The integral form histogram is divided into three regions, each fitted with a polynomial of different degrees. The degree of the polynomial for each region is chosen such that the χ^2 of the fit is minimized. The optimal configuration for fitting is to use the second degree polynomial for the low drift time region, the third degree polynomial for the center region and the forth degree polynomial for the high drift time region. This considerably increases the spatial resolution in comparison with the approach when the integral form is fitted by a straight line. The linear fit leads to spatial resolution of ~1cm while the desired resolution is of ~200 μm.

Transfer functions are defined per plane, due to observed differences in the planes behaviour. The reason for the different behaviour remains unknown and is still to be understood.

Having the distance reconstructed for a wire we need to decide at which side of the wire the particle passed. To resolve this right-left ambiguity the paired plane is used. If the fired wire number from first paired plane is N then the fired wire with number N or N+1 is the corresponding wire from the second paired plane. Having two possible coordinates on the first plane and two on the second we have four possible pairs. The pair that gives the smallest difference in terms of the spatial position is chosen as the true one and is used for further reconstruction steps. If no corresponding wires are found a double hit is reconstructed on a single plane because the right-left ambiguity cannot be resolved. The coordinates of the hits in this case will correspond to the coordinate of the wire ± the distance reconstructed out of this wire's time.

The spatial resolution of each double-plane can be estimated using the formula:

$$d_a + d_b - 5\ mm \tag{1}$$

Where d_a is the distance obtained from the wire signal on the first paired plane, d_b is the distance obtained from the wire signal on the second paired plane and 5 mm is the wire

position shift between the paired planes. The spatial resolution achieved by using the experimental data varies from 184 to 352 μm for different planes. The best result of 184 μm for the Y-oriented double plane is shown in Fig. 4.

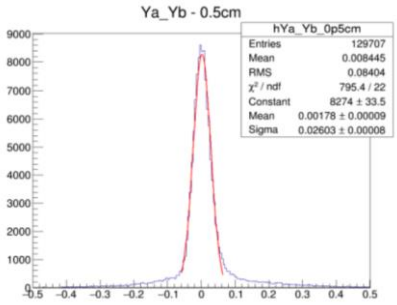

Fig. 4. Spatial resolution of the Y-oriented double plane.

Once all possible paired and single-plane coordinates are reconstructed they are assembled in segments. The segment reconstruction procedure is based on a simple algorithm. First a pair of X and Y coordinates is formed. U and V are rotated Cartesian coordinates and can be estimated by formulas:

$$U = \frac{Y-X}{\sqrt{2}}, V = \frac{X+Y}{\sqrt{2}}. \quad (2)$$

Knowing these estimates we look for them in the reconstructed set of coordinates. If we find a coordinate that is in proximity to the estimate we add it to the segment. The cuts on proximity in this case are chosen as 3*σ of the distribution of the difference between the reconstructed and estimated coordinates. On the first step only paired coordinates are considered. If we fail to add a paired coordinate from a particular double plane we look for single coordinates separately on each plane from the pair. This is because the quality of the paired coordinates is better, and are therefore given a higher priority.

The resulting segment is fitted in order to obtain its parameters, such as the slopes and global coordinates of the segment. To avoid high fake segment rates we require that a segment contains at least 6 points. The efficiency of each plane can be estimated analyzing the ratios of the missing hits on the reconstructed segments. It is presented on Fig. 5. The reconstruction efficiencies for all planes are around 90%. This is a good result concerning the age of these detectors.

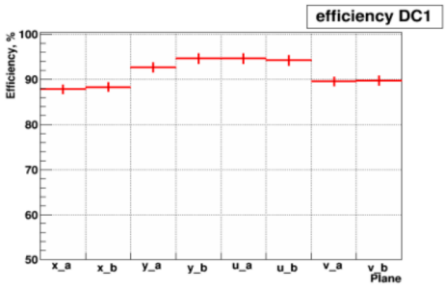

Fig. 5. Reconstruction efficiencies per plane.

The last reconstruction step consists in matching of a segment from the first chamber with a corresponding segment from the second chamber. Two segments must satisfy the cuts for the slope and global coordinate differences. The cuts correspond to 3*σ of the

overall slope and coordinate difference distributions. If they match these criteria they are assembled into a global track that is used further for global tracking and for linking the particle trajectory to ToF stations for its type identification.

MWPC DCH alignment

The local alignment of each detector system is performed in the same way. One detector out of the system is chosen as a reference one. First of all it is checked that the segments from different detectors of the same system have the same slope. After the needed adjustments with slopes are done we check if the global coordinates of the segments for the same z-coordinate coincide. If not, the coordinate is shifted in the needed direction by the value of the discrepancy.

The global alignment of the outer tracker is performed using the two detector systems described in the previous chapters. Experimental data with the analyzing magnet turned off are used for this purpose. In this case we have to deal with straight particle trajectories and the only deviations are caused by particles' interaction with materials from the experimental setup. The procedure is similar to the local alignment. The global position of the MWPC system is considered as the reference one, because the MWPC system is closer to the target and the particle meets less detector material on its way. First the global slopes of MWPC and DCH are compared and equalized. Afterward the global coordinates of the tracks from the two detector systems are equalized for z-coordinate of the target. The last step of the global alignment is vertex reconstruction using both detector systems. Besides the condition that there is no magnetic field in the analyzing magnet, a non-empty target is required for this purpose. If the global slopes and coordinates of the track in the target do not correspond with the required values, the whole system is shifted in order to eliminate the mismatch.

Beam momentum estimation

The quality of the global alignment of the outer tracker can be seen from the precision of the beam momentum estimation. When the beam passes through the magnetic field it curves. The two detector systems (MWPC and DCH) give us the incoming and outgoing angles. The beam momentum estimation procedure described in [4] is performed for the 4.5 GeV/nucleon carbon beam. The beam momentum is estimated for different values of the magnetic field integrals to give us a more general illustration of the method performance and alignment quality.

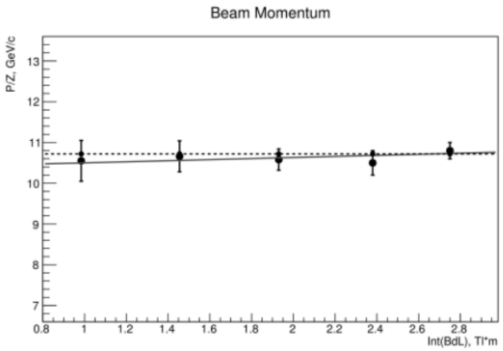

Fig. 6. C beam energy 4.5 GeV/nucleon momentum estimation. The dashed line is the nominal beam momentum value. The points are the beam momentum values estimated from experimental data.

The results are presented in Fig. 6. The nominal beam momentum value is represented by the dashed line on the picture. The data points fit with a solid line represent the values estimated from the experimental data. These points satisfy the nominal values within the statistical errors. The precision improves with the increase of the magnetic field integral due to the increase of the curvature. It can be seen from the values of the resolution that decrease from 4% to 2.2%. The resolution of 3% for the working values of the field integral is more than satisfactory and proves that the whole system can perform a very precise particle trajectory reconstruction.

Central tracker

The central tracker of the BM@N experiment comprises GEM detectors and double-sided silicon microstrip detectors. They are located inside the analyzing magnet and used to reconstruct the trajectory and momentum of charged particles. At present, it is only a part of the full configuration [1] designed to study Au - Au collisions. The full configuration (4 silicon and 7 GEM stations) is foreseen for 2021, when production of the GEM detectors at CERN [2] and microstrip Si stations at JINR and GSI will be completed.

Two coordinate triple-GEM detectors were chosen as a main component of the tracker. They sustain high rates of particles and stay operational in the strong magnetic field. Two types of GEM chambers were tested in the BM@N experiment: a smaller chamber with a size of 66x41 cm^2, and a larger one with a size of 1632x45 cm^2. In both types of detectors, signals are recorded from the anode plane using a double-side strip readout technique. Strips with a pitch of 800 μm were oriented at 0° and 15° with respect to the vertical axis. The readout board was divided into the outer and inner zones. Shorter strips were used in the inner (hot) zone located near the beam line to cope with a higher particle flux.

The operational parameters of the GEM detectors were chosen using simulations of electron shower propagation in a gaseous medium under electric field [5]. Simulations were confirmed by laboratory tests [6]. The technical run of the BM@N experiment was performed with a deuteron beam of 4 AGeV kinetic energy in December 2016 [7]. The central tracker for this run consisted of 5 small and 2 large GEM detectors. The beam was passing through the middle of the GEM planes in order to measure the efficiency and resolution with the beam particles and spectator protons and to have a maximum detector acceptance.

A relative momentum resolution of 9% and 6% was measured for beam deuterons with momenta of 9.7 GeV/c and for spectator protons with about a half of the deuteron momentum, respectively. A Λ hyperon signal was observed in the invariant mass spectrum of proton-π^- pairs in minimum bias beam interactions with different targets. All the tracker characteristics were found to be in good agreement with MC simulations.

The track reconstruction method was based on a cellular automaton approach [8]. Tracks found were used to reconstruct primary and secondary vertices using the "KF-particle" formalism [9]. Both (track and vertex) reconstruction packages were adapted from the CbmRoot software framework [10], where they were used for simulations of the Silicon Tracking System (STS) of the CBM detector.

In March 2017 the BM@N detector was operated in a carbon beam with kinetic energies from 3.5 to 4.6 AGeV to study inelastic interactions with C, Al and Cu targets. The central tracker was supplemented with a silicon station located 20 cm downstream from the target (Fig. 7). The station consisted of 8 modules with a full sensitive area of 25x25 cm^2. One module was composed of two silicon double sided microstrip detectors. Each detector had the sensitive area of 6.25x6.25 cm^2. The pitch sizes of vertical (Y) strips on the p+ side and oblique (2.5° to Y) strips on the opposite n+ side of the Si wafer were 95 μm and 103 μm, respectively. The primary vertex resolution along the beam direction for

minimum bias collisions improved from 2.8 cm in the deuteron beam run to 0.6 cm in the carbon beam run.

The goal of the current data analysis is a measurement of the dependency of the Λ hyperon yield on the rapidity and transverse momentum for different targets and beam energies. Monte Carlo simulations showed that ~4% of the Λ hyperons and 0.8% of K_S^0 could be reconstructed (these numbers will be much higher for the full configuration of the central tracker). Invariant mass spectra for $\Lambda \to p\pi^-$ decay candidates with soft and tight selection criteria on tracks and vertices are shown in Fig. 8. The main selection criteria included the proton-pion separation in the decay vertex (less than 8 and 6 mm for the soft and tight samples, respectively), lambda decay length (greater than 3.0 and 4.5 cm) and proton momentum (less than 4.3 and 3.0 GeV/c). The combinatorial background under the peak can be described by a second-degree polynomial on both spectra. This provides good conditions for the hyperon yield estimation. The mean value of the peak fits well to a Λ hyperon mass. The accurate central value obtained also confirms the quality of the magnetic field map used.

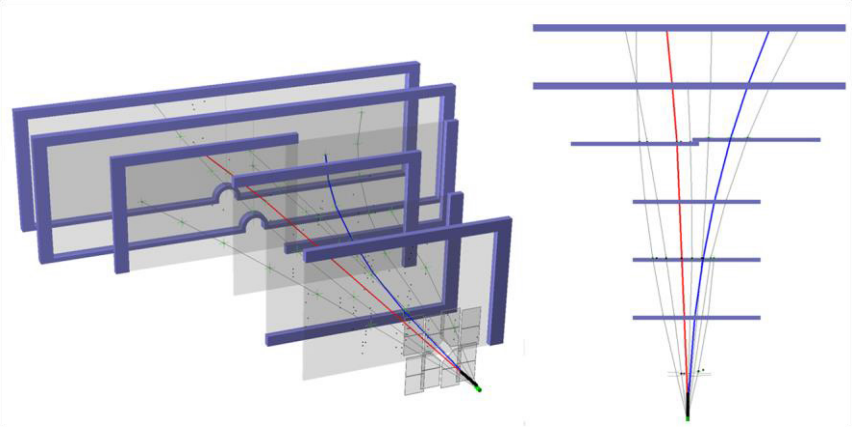

Fig. 7. Example of an event with $\Lambda \to p\pi^-$ decay candidate reconstructed in C+C collision.

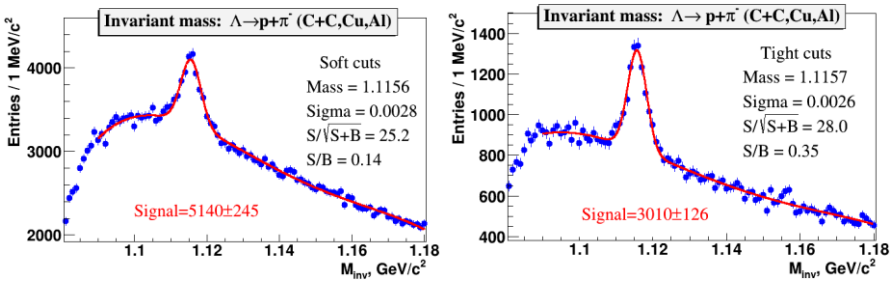

Fig. 8. Invariant mass spectrum of proton-π^- pairs reconstructed in interactions of a C beam of 4 AGeV energy with C,Al,Cu targets after applying soft (left) and tight (right) selection criteria on tracks and vertices selection.

The measurement of physical parameters of the Λ hyperon production requires precise estimates of the detectors' efficiency. Our analysis confirms very high efficiency (above 95%) of the GEM detectors except for the ±5 cm region close to the beam spot and at the edges of the GEM foil HV sectors occupying about 3% of the sensitive area. These parameters will be introduced into detailed Monte Carlo simulations to obtain the track reconstruction efficiency.

A significant step towards the complete configuration of the central tracker was made for the BM@N exposition in Ar and Kr beams with kinetic energies of 2.4-3.2 AGeV in March 2018. As it can be seen in Fig. 9 (left), 6 large GEM detectors were placed above the beam trajectory, so that beam particles passed through the chamber beam holes and did not irradiate detectors in contrast to the previous runs, since the GEM detectors and readout electronics could not be operated with the Ar/Kr beams crossing the detector sensitive area. Two additional small silicon stations with the sensitive area of 12.5x12.5 cm^2 were installed at distances of 10 and 12 cm downstream from the target. At present, the software alignment of the detector positions has been completed and the reconstruction of interactions of Ar and Kr beams with different targets has started. In minimum bias Ar+Cu collisions, a resolution of σ = 2 mm has been obtained for the Z-coordinate position of the primary vertex along the beam direction. For vertices with multiple reconstructed tracks (more than 5 tracks) the resolution is 1.1 mm.

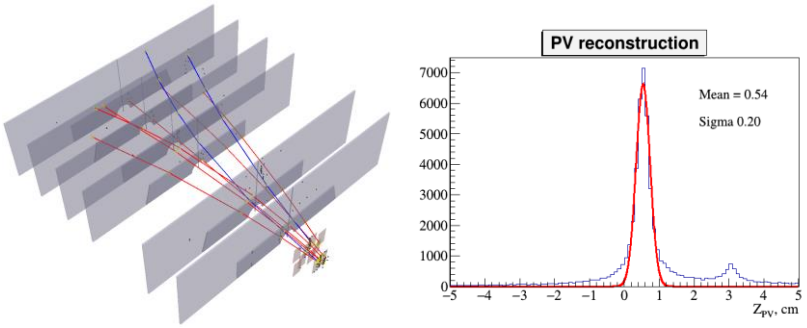

Fig. 9. Example of the reconstructed Ar+Cu collision (left). Distribution of the primary vertex position of Ar+Cu collisions along the beam direction (right).

Conclusion

First BM@N results on the Λ hyperon reconstruction were obtained with the initial detector configuration. The software for the main tracking detector systems was developed and commissioned. All systems showed good performance for different beams, targets and magnetic field values.

References

1. M.Kapishin, Eur.Phys.J., **A52**, 213 (2016);
2. F. Sauli, Nucl. Instrum. Meth., **A 805**, 2 (2016);
3. G.D. Barr et al., CERN/SPSC/90-22, 253 (1990);
4. N.Voytishin et al., EPJ-WoC, **173**, 04008 (2018);
5. D.Baranov and O.Rogachevsky, EPJ-WoC, **138**, 11004 (2017);
6. S.Bazylev et al., EPJ-WoC, **177**, 04004 (2018);
7. D.Baranov et al., Phys.Part.Nucl.Lett., **15**, 148 (2018);
8. V. Akishina, I. Kisel, J. Phys. Conf. Ser., **599**, 012024 (2015);
9. S. Gorbunov, I. Kisel, CBM-SOFT-note-2007-003 (2007);
10. http://cbmroot.gsi.de